nature genetics

The centrosomal protein nephrocystin-6 is mutated in Joubert syndrome and activates transcription factor ATF4

John A Sayer[1,2,22], Edgar A Otto[1,22], John F O'Toole[1], Gudrun Nurnberg[3,4], Michael A Kennedy[5], Christian Becker[3,4], Hans Christian Hennies[3,20], Juliana Helou[1], Massimo Attanasio[1], Blake V Fausett[6], Boris Utsch[1], Hemant Khanna[7], Yan Liu[8], Iain Drummond[8], Isao Kawakami[9], Takehiro Kusakabe[9], Motoyuki Tsuda[9], Li Ma[10], Hwankyu Lee[11], Ronald G Larson[11], Susan J Allen[1], Christopher J Wilkinson[12], Erich A Nigg[12], Chengchao Shou[13], Concepcion Lillo[14], David S Williams[14], Bernd Hoppe[15], Markus J Kemper[16], Thomas Neuhaus[16], Melissa A Parisi[17], Ian A Glass[17], Marianne Petry[18], Andreas Kispert[18], Joachim Gloy[19], Athina Ganner[19], Gerd Walz[19], Xueliang Zhu[10], Daniel Goldman[6], Peter Nurnberg[3,20], Anand Swaroop[7,21], Michel R Leroux[5] & Friedhelm Hildebrandt[1,21]

The molecular basis of nephronophthisis[1], the most frequent genetic cause of renal failure in children and young adults, and its association with retinal degeneration and cerebellar vermis aplasia in Joubert syndrome[2] are poorly understood. Using positional cloning, we here identify mutations in the gene *CEP290* as causing nephronophthisis. It encodes a protein with several domains also present in CENPF, a protein involved in chromosome segregation. CEP290 (also known as NPHP6) interacts with and modulates the activity of ATF4, a transcription factor implicated in cAMP-dependent renal cyst formation. NPHP6 is found at centrosomes and in the nucleus of renal epithelial cells in a cell cycle–dependent manner and in connecting cilia of photoreceptors. Abrogation of its function in zebrafish recapitulates the renal, retinal and cerebellar phenotypes of Joubert syndrome. Our findings help establish the link between centrosome function, tissue architecture and transcriptional control in the pathogenesis of cystic kidney disease, retinal degeneration, and central nervous system development.

Nephronophthisis (NPHP), a cystic kidney disease, is the most frequent genetic cause of chronic renal failure in children and young adults[1]. In Senior-Loken syndrome (SLSN) NPHP is associated with retinal degeneration. In Joubert syndrome (JBTS) NPHP is combined with retinal degeneration, cerebellar vermis aplasia, and mental retardation[2]. Identification of five genes mutated in NPHP[3–7] has implicated primary cilia[4,5,8], basal bodies[7] and mechanisms of planar cell polarity[9,10] in the pathogenesis of renal cystic disease[11]. However, it has remained unclear how this pathogenesis is mediated by downstream transcriptional events. In a worldwide cohort of 435 unrelated individuals with NPHP and isolated kidney involvement, 92 individuals with SLSN and 90 individuals with JBTS, recessive mutations of six known genes (*NPHP1*, *NPHP2*, *NPHP3*, *NPHP4*, *IQCB1* (also known as *NPHP5*), and *AHI1*) were detected only in 35% of purely renal NPHP cases, in 21% of SLSN cases[7], and in 1% of JBTS cases[12]. To identify further causative genes for NPHP, we performed a whole-genome search for linkage by homozygosity mapping using the 10K Affymetrix SNP array.

We analyzed 25 consanguineous kindreds with NPHP, SLSN, or JBTS, ascertained worldwide, each of which had two affected individuals and was negative for mutations in known *NPHP* genes. Three kindreds showed an overlap of nonparametric lod score (NPL) peaks on chromosome 12q that indicated potential homozygosity by

[1]Department of Pediatrics, University of Michigan, Ann Arbor, Michigan 48109, USA. [2]Institute of Human Genetics, School of Clinical Medical Sciences, University of Newcastle upon Tyne, NE1 3BZ, UK. [3]Cologne Center for Genomics, University of Cologne, Cologne, Germany. [4]RZPD Deutsches Ressourcenzentrum fuer Genomforschung GmbH, Berlin, Germany. [5]Department of Molecular Biology and Biochemistry, Simon Fraser University, Burnaby, British Columbia V5A 1S6, Canada. [6]Molecular and Behavioral Neuroscience, Institute and Department of Biological Chemistry, University of Michigan, Ann Arbor, Michigan 48109, USA. [7]Department of Ophthalmology, University of Michigan, Ann Arbor, Michigan 48109, USA. [8]Harvard Medical School and Renal Unit, Massachusetts General Hospital, Charlestown, Massachusetts 02129, USA. [9]Department of Life Science, Graduate School of Life Science, University of Hyogo, Hyogo 678-1297, Japan. [10]Institute of Biochemistry and Cell Biology, Shanghai Institutes of Biological Sciences, Shanghai 200031, China. [11]Departments of Biomedical Engineering and Chemical Engineering, University of Michigan, Ann Arbor, Michigan 48109, USA. [12]Max-Planck Institute for Biochemistry, Department of Cell Biology, D-82152 Martinsried, Germany. [13]Department of Biochemistry and Molecular Biology, Peking University School of Oncology, Beijing Institute for Cancer Research, Beijing 100036 PRC, China. [14]Departments of Pharmacology and Neurosciences, School of Medicine, University of California at San Diego, La Jolla, California 92093-9012, USA. [15]Department of Pediatrics, University of Cologne, Cologne, Germany. [16]Department of Pediatrics, University of Zurich, Zurich, Switzerland. [17]Department of Pediatrics, University of Washington, Seattle, Washington 98105, USA. [18]Institute for Molecular Biology, Medizinische Hochschule Hannover, D-30625 Hannover, Germany. [19]University of Freiburg, Freiburg, Germany. [20]Institute for Genetics, University of Cologne, Cologne, Germany. [21]Department of Human Genetics, University of Michigan, Ann Arbor, Michigan 48109, USA. [22]These authors contributed equally to this work. Correspondence should be addressed to F.H. (fhilde@umich.edu).

Received 19 December 2005; accepted 21 March 2006; published online 7 May 2006; doi:10.1038/ng1786

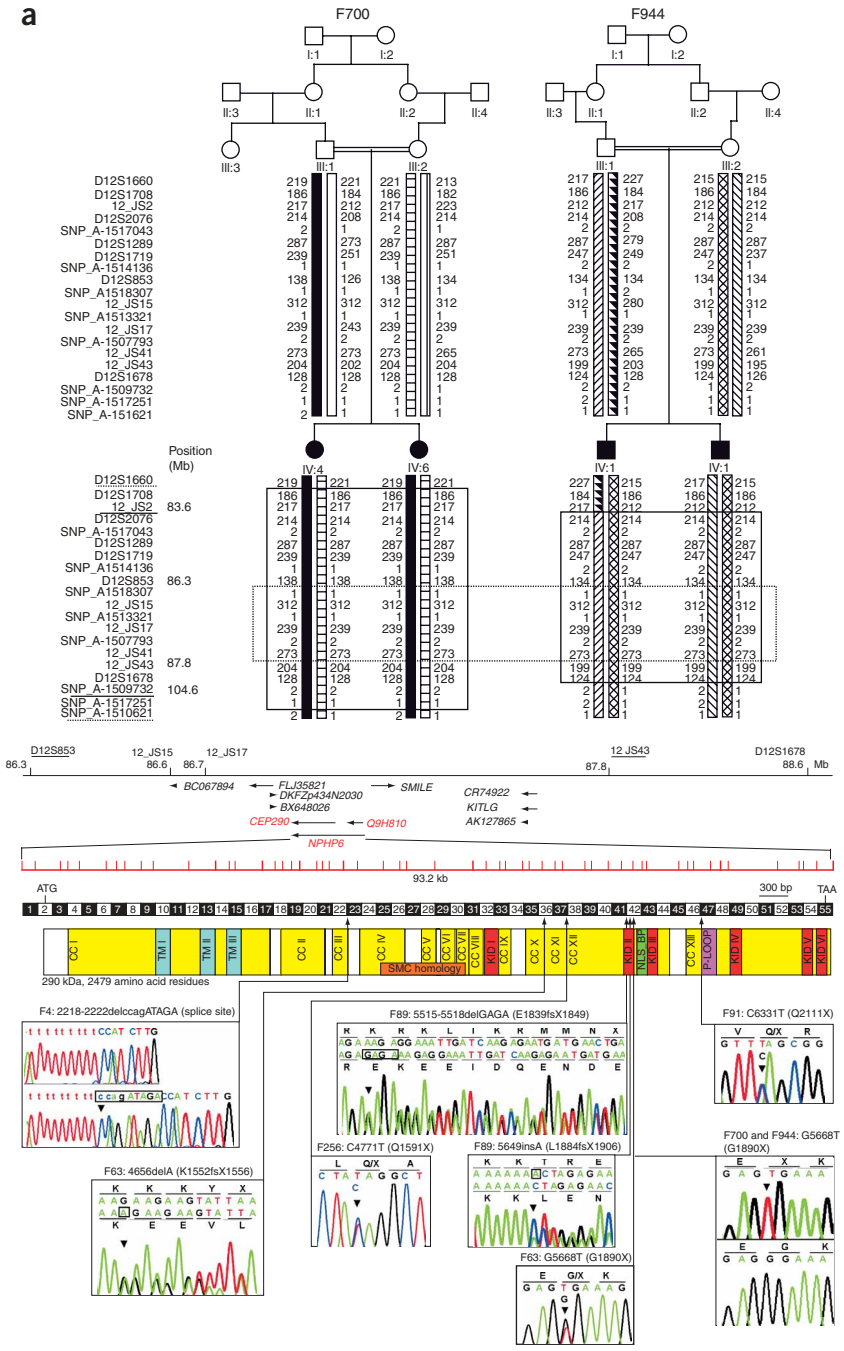

Figure 1 Positional cloning of the *CEP290* gene as mutated in NPHP6/SLSN6/JBTS6. (**a**) Haplotype analysis in two consanguineous kindreds. Microsatellite and SNP markers on chromosome 12q are shown at left (top to bottom, centromere to q-terminal). Boxes with solid lines indicate the extent of homozygosity by descent. Haplotype sharing occurs among both families within a 1.5-Mb interval on chromosome 12q21.32-q21.33 (box with dotted line). This defines a critical interval for a putative *NPHP6/SLSN6/JBTS6* locus under the hypothesis of haplotype sharing by descent from a postulated ancestor common to F700 and F944. Circles represent females; squares represent males; filled symbols denote the presence of JBTS. (**b**) The *NPHP6* critical genetic region, as annotated by GenomeBrowser (UCSC May 2004 freeze), extends over a 1.5-Mb interval between flanking markers *D12S853* and *12_JS43* (underlined). Arrows indicate transcriptional direction of all ten positional candidate genes. Mutations were detected in the partially annotated gene *CEP290*, which was found to be part of a larger gene (including *Q9H8I0* and additional exons). This re-annotated gene is now termed *CEP290* (alias *NPHP6*). (**c**) The *CEP290* gene measures 93.2 kb and extends over 55 exons (vertical hatches). (**d**) Exon structure of human *CEP290* cDNA. Exon size, which ranged from 21 bp to 465 bp, is averaged graphically. (**e**) Representations of putative protein motifs shown in relation to the position of the exons encoding them. Lines and arrows indicate relative positions of the mutations detected. Protein domains are numbered and marked as follows: CC, coiled-coil domain; TM, tropomyosin homology domain; KID, RepA/Rep$^+$ protein KID; NLS_BP, bipartite nuclear localization signal; P-loop, ATP/GTP-binding site motif A (P-loop). The extent of homology with SMC proteins is indicated by an orange bar. (**f**) Nine different *NPHP6* mutations were detected in seven families with NPHP/JBTS and one family with SLSN. Family number and mutations (see **Table 1**) are given above sequence traces. Mutated nucleotide and amino acid sequence letter codes are shown above, and wild-type, below. For homozygous mutations, wild-type sequence is shown below mutated sequence. Deletions or insertions are highlighted in boxes with mutated sequences. The deletion in F4 is highlighted in wild-type sequence. Mutation G1890X is shown in both the homozygous and heterozygous states. Mutations for A197 are not shown for reasons of space.

descent (**Supplementary Fig. 1** online). Kindred F944 established an interval of homozygosity (21.0 Mb) between markers *12_JS2* and *SNP_A_1509732* (**Fig. 1a**). Under the hypothesis of a shared haplotype from a common ancestor of kindreds F700 and F944, we refined the critical region to nonshared markers *D12S853* and *12_JS43* within a 1.5-Mb interval (**Fig. 1a**), thereby identifying a putative locus (*NPHP6/SLSN6/JBTS6*) for NPHP, SLSN, or JBTS on chromosome 12q21.32-q21.33. Upon mutational analysis within the *NPHP6* genetic interval (**Fig. 1**), we identified an identical homozygous nonsense mutation, 5668G>T (G1890X; **Table 1** and **Fig. 1f**), in both kindreds (F700 and F944) that segregated with the affected status in a partially annotated gene (*CEP290*), which had been described as a component of the centrosomal proteome[13]. We performed mutational screening in a total of 96 unrelated individuals with JBTS by direct sequencing of all 55 exons, which we predicted from EST clones that made up the full-length *CEP290* cDNA (**Fig. 1c,d**; **Supplementary Fig. 2** online; detailed exon structure available from authors). Altogether, we identified nine distinct *CEP290* mutations in seven families with JBTS and one family with SLSN (**Table 1** and **Fig. 1f**). Interestingly, all sequence changes were nonsense or frameshift mutations. In two families, we found only one heterozygous mutation in each family (**Table 1** and **Fig. 1f**). We did not detect any mutations in >190 chromosomes of healthy controls. We thus identified mutations in *CEP290* as the cause of JBTS or SLSN. In analogy to genes previously identified as mutated

Table 1 Nine different *NPHP6* mutations detected in seven families with JBTS and one family with SLSN

Family (individual)	Origin	Nucleotide alteration(s)[a]	Alteration(s) in coding sequence	Exon (segregation)[b]	Parental consanguinity	Age at ESRD[c] (in years)	Ocular symptoms (age of onset in years)	Central nervous system symptoms (other)
F4 (II-1)	Turkey	2218-2222del ccagATAGA	obligatory splice site	23 (splice donor) (hom, M, P)	+	11	TRD (reduced vision <3)	ND
(II-2)						13	TRD (reduced vision <2)	ND
F63 (II-1)	Germany	4656delA, G5668T	K1552fsX1556, G1890X	36 (het, M) 41 (het, P)	–	12	CA, NY, early-onset TRD	CVA, AT, MR, MEC, cystic orbital tumor, (scoliosis)
A197 (II-1)	Denmark	7341-7342insA, 3175-3176insA	L2448fsX2455, I1059fsX1069	55 (het, ?) 29 (het, ?)	–	Normal at 9.5 yrs	CA, RC, early-onset TRD	CVA, AT, MR
F256 (II-1)	USA	C4771T ?	Q1591X, ?	37 (het, P)	–	<18	CA, NY	CVA, AT, MR
(II-4)						5	CA, NY	CVA, AT, MR
F89 (II-1)	Germany	5515-5518delGAGA, 5649insA	E1839fsX1849, L1884fsX1906	41 (het, M) 42 (het, P)	–	11	CA, NY	CVA, AT, MR
F700 (III-4)	Turkey	G5668T	G1890X	42 (hom, M, P)	+	11	TRD <11 yrs,	CVA, AT, MR
(III-6)						>2 months[d]	NY CA, NY	CVA, AT, MR, MEC
F944 (III-1)	Turkey	G5668T	G1890X	42 (hom, M, P)	+	>13[d]	ND	CVA, AT
(III-2)						>11[d]	ND	CVA, AT
F91 (II-1)	Germany	C6331T, ?	Q2111X, ?	47 (het, *de novo*)	–	10	CA, NY, RC	CVA, AT, MR

AT, ataxia; CA, congenital amaurosis (bilateral); CVA, cerebellar vermis aplasia/hypoplasia; ESRD, end-stage renal disease; ND, no data available; NY, nystagmus; RC, retinal coloboma; TRD, tapetoretinal degeneration; MEC, occipital menigoencephalocele; MR, mental retardation or psychomotor retardation; ?, second mutation not detected. [a]All mutations were absent from at least 190 chromosomes of healthy controls. [b]het, heterozygous in affected individual; hom, homozygous in affected individual; M, mutation identified in mother; P, mutation identified in father; nd, no data or DNA available. [c]All patients had renal ultrasonography results compatible with NPHP (increased echogenicity and/or corticomedullary cysts). [d]Renal function significantly reduced.

in NPHP[3–7], we termed this gene *CEP290* (also known as *NPHP6*, *SLSN6* and *JBTS6*). All of the affected individuals, including those from families F700 and F944, but with the exception of family F4 with SLSN, showed renal ultrasonographic and clinical features of JBTS (**Table 1**). In family F197 there was no renal involvement. The *CEP290* gene, which encodes nephrocystin-6 (NPHP6), spans 55 exons and 93.2 kb on human chromosome 12q21.32 (**Fig. 1b,c**). RNA blot analysis demonstrated a major *CEP290* transcript of approximately 8 kb that is expressed strongly in placenta and weakly in brain (data not shown). The 290-kDa NPHP6 protein (2,479 amino acid residues) is encoded within the human full-length *CEP290* mRNA of 7,951 nt (**Fig. 1d**).

Analysis of the deduced NPHP6 amino acid sequence (**Supplementary Fig. 3** online; **Fig. 1e**) yielded 13 putative coiled-coil domains, a region with homology to SMC (Structural Maintenance of Chromosomes) chromosome segregation ATPases[14], a bipartite nuclear localization signal (NLS_BP), six RepA/Rep$^+$ protein KID motifs (KID), three tropomyosin homology domains and an ATP/GTP binding site motif A (P-loop). Although NPHP6 is unique within human protein databases, the kinetochore protein CENPF contains an essentially identical set of putative domains, although they are distributed in a different order along the protein sequence (data not shown). CENPF has a role in chromosome segregation during mitosis and associates with the nuclear matrix in interphase[15]. The SMC1 and SMC3 proteins have recently been shown to directly interact with the retinitis pigmentosa GTPase regulator (RPGR)[16], a protein expressed in primary cilia and centrosomes that is mutated in 15–20% of individuals with retinitis pigmentosa. RPGR participates in a complex with nephrocystin-5, which is mutated in NPHP5 type 5 (ref. 7). A bipartite nuclear localization signal is also found in inversin (nephrocystin-2), which is mutated in NPHP type 2 (ref. 5). There are six RepA/Rep$^+$ protein motifs KID (KID) that exist in the proteins CENPE, CENPF, SMC1L1, SYNE2 and dystonin, some of which are involved in chromosome segregation and cell cycle regulation. All of the predicted motifs of human NPHP6 are highly conserved in the evolutionarily distant organism *Ciona intestinalis* (sea squirt) ortholog nphp6 (*ci0100142505*; 36% amino acid identity), suggesting a conserved function of the domain assembly within NPHP6 (data not shown).

Proteins involved in renal cystic disease such as nephrocystin-1, nephrocystin-2 (inversin)[5,17], nephrocystin-4 (refs. 6,18) and nephrocystin-5 (ref. 7) have been shown to localize to primary cilia, centrosomes and adherens junctions of renal epithelial cells in a cell cycle–dependent manner[8]. A monoclonal antibody (3G4)[19] directed against NPHP6 recognized in immunoblots the endogenous and overexpressed full-length NPHP6 of 290 kDa when expressed in HEK293 cells (**Supplementary Fig. 4** online). A second monoclonal antibody against NPHP6 (4H9)[19] was similarly specific (data not shown). Upon immunofluorescence microscopy of ciliated kidney IMCD3 cells, the 3G4 antibody detected endogenous NPHP6 within centrosomes and colocalized with the centrosomal protein marker γ-tubulin (**Fig. 2a**). We also observed this same immunostaining pattern in nonciliated COS-7 cells (**Supplementary Fig. 5** online) and with the 4H9 antibody to NPHP6 (**Supplementary Fig. 5** online). We did not detect NPHP6 along ciliary axonemes in IMCD3 cells. Treatment of IMCD3 cells with nocodazole (25 μM) for 1 h, which disrupts the microtubule architecture, did not affect the association of NPHP6 with the centrosome in either IMCD3 cells (**Fig. 2b**) or COS7 cells (**Supplementary Fig. 5** online). This suggests that NPHP6 is not bound to the minus ends of microtubules, which are loosely associated with the centrosome. Furthermore, overexpression of p50-dynamitin, an antagonist of dynein-dynactin motor function[20], did not result in lack of trafficking of NPHP6 to the centrosome (**Supplementary**

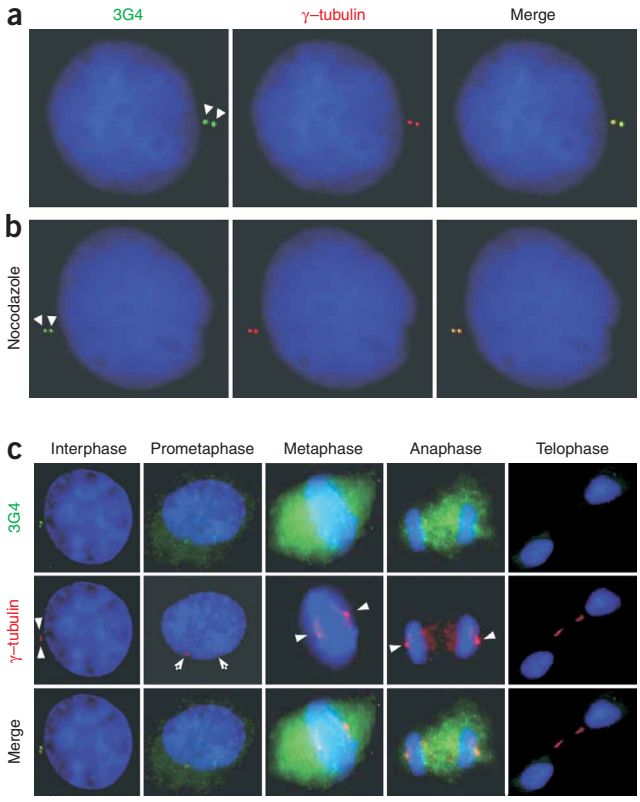

Figure 2 NPHP6 localizes to the centrosome during interphase, independent of microtubule polymerization. (**a**) Coimmunofluorescence staining in IMCD3 cells using an antibody against endogenous NPHP6, 3G4 (green), shows distinct perinuclear staining of NPHP6 colocalizing at the centrosomes (arrowheads) with the centrosomal marker γ-tubulin (red). (**b**) Treatment of IMCD3 cells with the microtubule depolymerizing agent nocodazole did not affect the colocalization of NPHP6 (3G4, green) with γ-tubulin (red). (**c**) NPHP6 demonstrates a dynamic localization throughout the cell cycle. Colocalization of NPHP6 (3G4, green) with γ-tubulin (red) became less evident in prometaphase, and NPHP6 was present diffusely throughout the cytoplasm at later stages of cell division. Cell cycle stages are indicated in each panel. Nuclei are stained blue with DAPI. Signal strength of 3G4 does not reflect relative amounts of NPHP6 when compared between cell cycle stages.

Fig. 6 online). Together, these results indicate that, as with other integral centrosomal components such as γ-tubulin, NPHP6 centrosomal localization occurs in a microtubule- and dynein-independent manner[21]. Furthermore, NPHP6 localization to the centrosome is dynamic, as the protein redistributes to the cytosol starting in prometaphase, similar to the localization of other proteins involved in renal cystic disease[17,22] (**Fig. 2c**). The retina harbors a structure analogous to the primary cilium, termed the photoreceptor connecting cilium[23]. As all individuals carrying *CEP290* mutations had early-onset retinal degeneration or coloboma, we examined the distribution of NPHP6 by immunogold labeling of mouse photoreceptor cells. NPHP6 showed its greatest concentration in the connecting cilium of mouse photoreceptor cells (**Supplementary Fig. 7** online), thereby supporting a possible ciliary role in the eye[7].

We examined *cep290* expression in developing zebrafish by *in situ* hybridization (**Fig. 3**), detecting expression in the tail of embryos 24 h post-fertilization (hpf) in a caudal-to-rostral gradient and at lower levels in the cerebellum (**Fig. 3a**) and retina (**Fig. 3b**). At 48 hpf, *cep290* was strongly expressed at the boundary between the developing cerebellum and tectum (**Fig. 3g**, black arrow) and in the retina with strong expression near the lens (**Fig. 3g**, white arrow). Loss-of-function examined by antisense morpholino oligonucleotide injection targeting the *cep290* ATG initiation codon (atgMO) and an internal splice donor sequence (exon 42, spMO) both caused defects in retinal, cerebellar, and otic cavity development (**Fig. 3c–f,h–j**) as well as cyst formation in the pronephric kidney tubules (**Fig. 3k–n**). These phenotypes are markedly similar to the clinical features seen in the individuals with JBTS (**Table 1**). In fact, ectopic tissue in the fourth ventricle (**Fig. 3i**, arrowhead) and lack of some retinal tissue (**Fig. 3i**, arrow) resemble the meningoencephalocele and retinal coloboma, respectively, observed in some individuals with JBTS (**Table 1**). A mismatch control morpholino (mmMO) had no effect on nervous system development or renal cyst formation, suggesting specificity for the knockdown (**Fig. 3d,e,h**). We observed developmental defects of the nervous system in separate injections with varying penetrance (atgMO: 23/53, 43%; spMO: 22/67, 33%). We also observed kidney cyst formation consistently in separate injections (atgMO: 43/92, 47%; spMO: 18/57, 32%; **Fig. 3k–n**). The localization of cep290 to the centrosome and the association of ciliary defects with cystic kidney defects prompted us to examine cilia in embryos with cystic pronephroi[24]. Notably, we did not observe any defects in cilia length (data not shown) or motility (**Supplementary Videos 1** and **2** online).

To shed further light on the role of NPHP6 in early embryonic development, we performed *in situ* expression analyses and morpholino knockdown studies on *Ciona intestinalis* (**Fig. 4**). *nphp6* transcripts were present in eggs and cleavage-stage embryos as maternal mRNA. At the eight-cell stage, *nphp6* was expressed in A4.2 blastomeres, which later give rise to anterior brain and epidermis (**Fig. 4a**). Later in embryogenesis, we detected *C. intestinalis nphp6* expression in anterior dorsal tissues (**Fig. 4b,c**) and at the tailbud stage in ectoderm cells of the forming tailbud (**Fig. 4d**). At the swimming larva stage, expression was observed in the oral siphon rudiment, the atrial siphon rudiments and a small portion of the anterior central nervous system (**Fig. 4e**). These cranial sensory placodes are anlagen of adult sensory organs and during metamorphosis will be the sites of active cell division and morphogenesis[25].

To identify direct interaction partners of NPHP6, we performed a yeast two-hybrid screen of a human fetal brain expression library using an NPHP6 construct encoding exons 2-21 as 'bait' (**Supplementary Fig. 2** online). The screen yielded ATF4 as a direct interaction partner of NPHP6. The interaction of NPHP6 with ATF4 was further confirmed by a direct yeast two-hybrid assay after switching 'bait' and 'prey' (**Fig. 5a**) as well as by coimmunoprecipitation (see below). We used this N-terminal construct to partially map the protein interaction domain on NPHP6 to its N-terminal third encoded by exons 2–21 (**Supplementary Fig. 2** online). It was also mapped to the C-terminal two-thirds of ATF4, as the shortest ATF4 clone identified in the yeast two-hybrid screen extends from amino acid 138 to the stop codon (at codon 352). To confirm that NPHP6 and ATF4 interact physiologically *in vivo*, we performed coimmunoprecipitation experiments using bovine retina extracts. Immunoblot analysis demonstrated that endogenous ATF4 can be immunoprecipitated using an antibody to NPHP6 but not using a control IgG (**Fig. 5b**). Reverse coimmunoprecipitation experiments showed that antibody to ATF4 can also precipitate endogenous NPHP6 (**Fig. 5c**).

The centromeric protein CENPF, which harbors the same content of putative protein domains as NPHP6, has also been shown to directly interact with ATF4 (ref. 15). To understand the functional

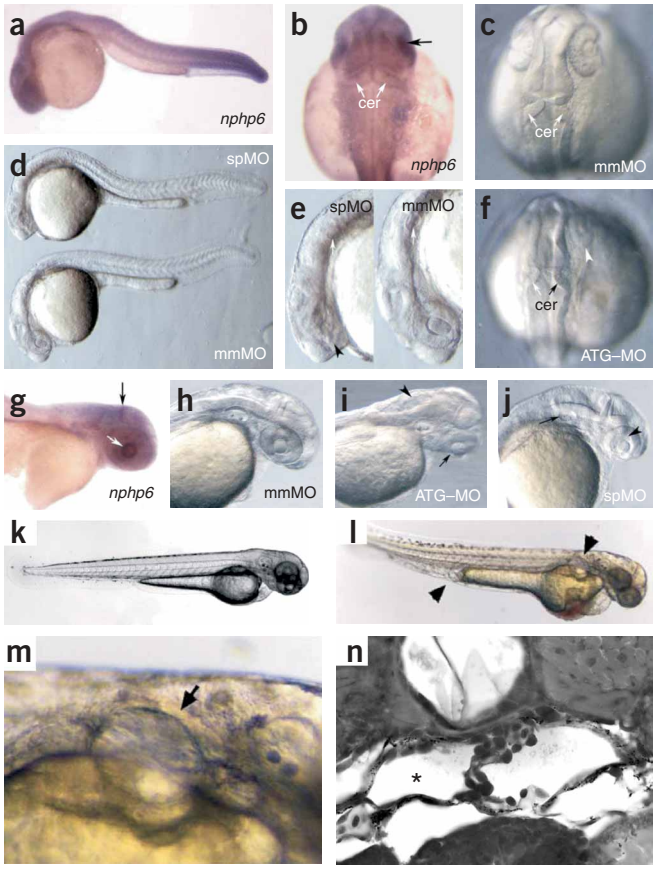

Figure 3 *nphp6* expression pattern and targeted knockdown of zebrafish *nphp6* are consistent with the kidney, cerebellar and retinal phenotypes of Joubert syndrome. (**a**–**f**) *nphp6* expression and targeted knockdown at 24 hpf. (**a**) *nphp6* is strongly expressed in the tail of 24- to 30-hpf larva and is expressed throughout the central nervous system at lower levels. (**b**) Dorsal view of *nphp6* expression in 30 hpf larva. The outer edges of the developing cerebellum express *nphp6* (white arrows). The retina near the lens also expresses *nphp6* (black arrow). (**c**) Mismatch morpholino (mmMO)-injected larva at 24 hpf showing normal development of the cerebellum (arrows) and eyes. (**d**,**e**) Splice site (spMO)- and mmMO-injected larvae at 24 hpf. (**d**) A low-magnification view of spMO and mmMO larvae shows that much of the body develops normally in mmMO-injected larvae. (**e**) Higher magnification of larvae shown in **d** demonstrates that the spMO larva has a much smaller eye (black arrowhead) and lower brain mass than the mmMO larva. The spMO larva also has a highly underdeveloped otic cavity (white arrows), the precursor to the zebrafish ear. (**f**) Start codon morpholino (ATG-MO)-injected larva at 24 hpf with marked reduction in eye size (white arrowhead) and cerebellar development (white arrow). The right side of the cerebellum does not fold properly (black arrow). cer, cerebellum. (**g**–**j**) *nphp6* expression and morpholino-induced defects in cerebellar, retinal and otic cavity development at 48 hpf. (**g**) *nphp6* is strongly expressed at the boundary between the cerebellum and tectum (black arrow) and in the retina near the lens (white arrow) at 48 hpf. (**h**) mmMO-injected larva at 48 hpf. (**i**) atgMO larva with ectopic brain tissue in the fourth ventricle (arrowhead) and reduced eye size (arrow) compared with mmMO larva. (**j**) spMO larva with defects in retinal development visible as a gap between the lens and retina (arrowhead) and reduced otic cavity size (arrow). (**k**–**n**) *nphp6* loss of function in zebrafish results in pronephric cysts. (**k**) Wild-type zebrafish larva at 2.5 days post-fertilization (dpf). (**l**) *nphp6* ATG-MO (0.5 mM)-injected embryo showing cyst formation in the pronephric tubule and glomerulus and defects in cloaca formation (arrowheads). (**m**) Enlarged view of pronephric cyst formation (arrow). (**n**) Enlarged view of histological section of distended pronephric tubules (asterisk) in *nphp6* morphants at 2.5 dpf.

relevance of the interaction between NPHP6 and ATF4, we examined effects of NPHP6 overexpression on the transactivation activity of ATF4. We used the *myc*-tagged full-length NPHP6 clone (pCJW206-Cep290, or NPHP6-*myc*), which showed correct centrosomal localization (**Supplementary Fig. 6** online), in cotransfection experiments with a full-length ATF4 clone (pCEP-ATF4) to assess the activation of a dual-luciferase reporter construct for ATF4 (pCRE-ATF4X2) in HEK293T cells (**Fig. 5d**). Compared with transfection with the empty vector pCEP4F, expression of *myc*-CEP290 or ATF4 alone had only a small effect on reporter activity (a roughly twofold increase); however, cotransfection of both NPHP6 and ATF4 constructs strongly increased reporter activity (9.7-fold) (**Fig. 5d**). These results indicate that NPHP6 activates ATF4-mediated transcription. Notably, it also suggests that NPHP6 antagonizes the function of CENPF, which also binds but instead represses the activity of ATF4 in dual-luciferase assays[15].

The RNA interference construct pTER-NPHP6 was able to completely silence exogenous *myc-NPHP6* in HEK293T cells upon cotransfection (data not shown). It generally knocked down endogenous levels of NPHP6 protein by 73% for 48 h upon transfection (**Fig. 5e**), comparable to the ~80% transfection efficiency obtained when using green fluorescent protein (GFP) as a marker. When pTER-NPHP6 was cotransfected with the reporter construct pCRE-ATF4X2 into HEK293T cells, it suppressed the reporter activity by 75.4% compared with empty vector (**Fig. 5f**), probably as a result of disrupting endogenous NPHP6 function. This further supports the notion that NPHP6 can activate ATF4-mediated transcription. Endogenous as well as GFP- or myc-tagged ATF4 showed nuclear localization by immunofluorescence microscopy in COS7 cells (data not shown but available from authors) and IMCD3 cells (data not shown). NPHP6 contains a nuclear localization signal (**Fig. 1e**; **Supplementary Fig. 3** online) and therefore was expected to show at least partial nuclear localization in order to activate ATF4. To explore this possibility, we subjected HEK293T cells to subcellular fractionations. CENPF (mitosin) and α-tubulin were used as markers for nuclear and cytoplasmic fractions, respectively. Consistently, NPHP6 showed nuclear localization in addition to cytoplasmic localization (**Fig. 5g**). We obtained similar results in HeLa cells (data not shown).

In this study, we identify a previously unknown centrosomal protein, nephrocystin-6 (NPHP6), that is disrupted in Joubert syndrome. Our finding that NPHP6 interacts physically with and activates ATF4 generates the first example of downstream signaling components on the level of transcriptional regulation in this disease group.

Note added in proof: Recently, a Cep290 in-frame deletion in the mouse model rd16 was found to cause retinal degeneration without renal or cerebellar involvement[30].

METHODS

Subjects. We obtained blood samples and pedigrees after obtaining informed consent from individuals with NPHP and/or their parents. Approval for experiments on humans was obtained from the University of Michigan Institutional Review Board. In all affected individuals, the diagnosis of nephronophthisis was based on the following criteria: (i) clinical course and renal ultrasound or renal biopsy were compatible with the diagnosis of NPHP/SLSN/JBTS as judged by a (pediatric) nephrologist and (ii) individuals had entered end-stage renal disease, with the exception of F197, in whom kidney disease was absent at age 9.5 years. Retinal degeneration or retinal coloboma were diagnosed by an ophthalmologist. Criteria for Joubert syndrome were based on the following clinical minimal criteria: (i) nephronophthisis (except

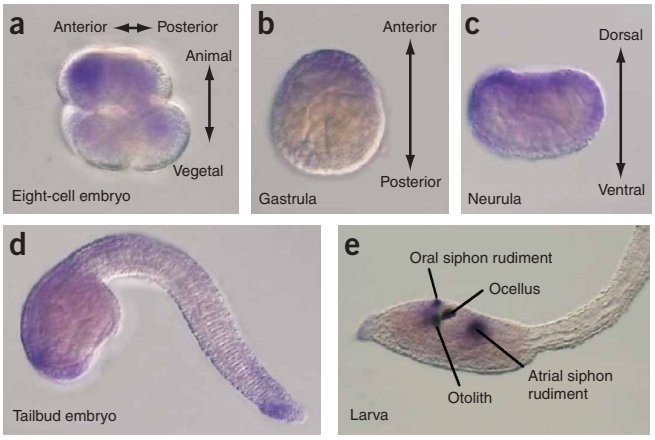

Figure 4 The *cep290* homolog of *C. intestinalis* shows a dynamic developmental expression pattern and results in developmental arrest upon targeted knockdown. (**a**–**e**) Expression of *cep290* in *C. intestinalis* eight-cell embryo (**a**), gastrula (**b**), neurula (**c**), tailbud embryo (**d**) and larva (**e**). (**a**–**c**) *cep290* transcripts are present in eggs and cleavage-stage embryos as maternal mRNA. In cleavage stage embryos they show a localized distribution pattern. At the eight-cell stage (**a**), transcripts are predominantly localized in a4.2 blastomeres, which mainly produce anterior brain and epidermis. They are less abundant in A4.1, B4.1 and B4.2 blastomeres. (**b**,**c**) In later embryogenesis, the *C. intestinalis cep290* mRNA is predominantly expressed in the anterior dorsal part of the embryo. (**d**) At the tailbud stage there is also expression in ectoderm cells of the prospective tailbud of the neurula. At the swimming larva stage (**e**), *C. intestinalis* nphp6 is expressed in three specific regions of the larva: the oral siphon rudiment, the atrial siphon rudiments and a small portion of the anterior central nervous system. These cranial sensory placodes are anlagen of adult sensory organs.

F197); (ii) congenital amaurosis, retinal degeneration or coloboma and (iii) presence of cerebellar vermis aplasia/hypoplasia and/or cerebellar ataxia/hypotonia. Nystagmus, oculomotor apraxia and psychomotor or developmental delay were optional symptoms.

Linkage and mutational analysis. For genome-wide homozygosity mapping, the 10K Affymetrix SNP array was used to perform a total genome search for linkage in 25 consanguineous families with NPHP, SLSN or JBTS. Data was evaluated by performing nonparametric lod scores (NPL) across the whole genome in order to identify regions of homozygosity. Areas of homozygosity were confirmed by performing high-resolution haplotype analysis within the identified regions. Published microsatellite markers as well as newly designed markers were used. Additional SNPs were typed by direct sequencing. The GENEHUNTER program was used to calculate multipoint lod scores assuming recessive inheritance with complete penetrance, a disease allele frequency of 0.001 and marker allele frequencies of 0.125. Exon primers used for PCR and direct sequencing of all 55 *CEP290* exons are given in **Supplementary Table 1** online.

***In situ* hybridization of *C. intestinalis cep290*.** A digoxigenin-labeled antisense riboprobe was synthesized from a 1.3-kb *C. intestinalis cep290* cDNA corresponding to the 3′ end of the gene cloned in a pBluescript vector using T7 RNA polymerase. Whole-mount *in situ* hybridization was performed as previously described[26].

***In situ* hybridization of zebrafish *cep290*.** Sense and antisense digoxigenin-labeled riboprobes were synthesized from linearized pBluescript vector

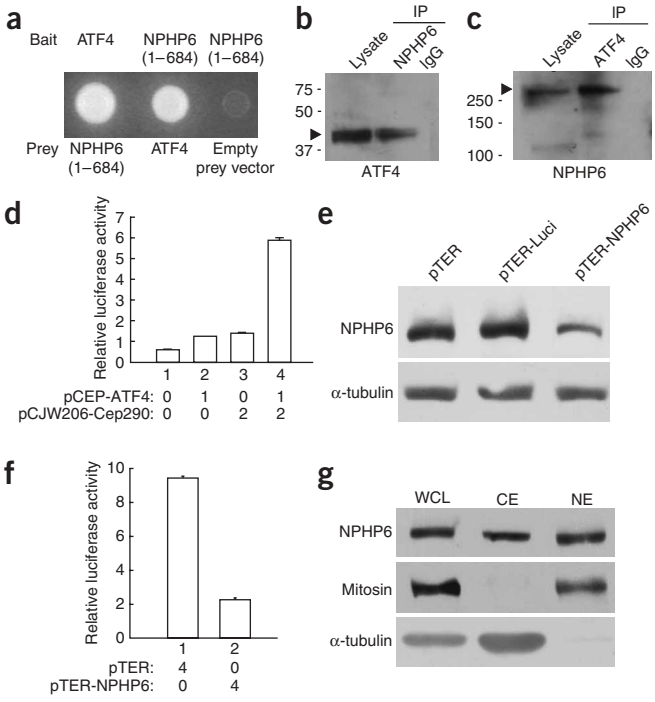

Figure 5 NPHP6 partially localizes to the nucleus, directly interacts with ATF4 and induces its transcriptional activation. (**a**) A human fetal brain yeast two-hybrid expression library was screened with a partial NPHP6 clone (residues 1–684) fused with the DNA-binding domain of the GAL4 protein (pDEST 32) bait vector yielding ATF4 as a direct interaction partner of NPHP6. Interaction was retested in a direct yeast two-hybrid assay after recloning ATF4 into another prey vector; (**a**, middle colony), and after switching bait (pDEST32) and prey (pDEST22) vectors (**a**, left colony). Empty vector control was negative (**a**, right colony). (**b**,**c**) Coimmunoprecipitation of NPHP6 with ATF4 from bovine retina. Immunoprecipitation (IP) from bovine retinal extracts (500 μg) was performed using anti-NPHP6 (3G4), anti-ATF4 or normal rabbit immunoglobulin (IgG). Immunoblots were developed using antibody to ATF4 (**b**) or antibody to NPHP6 3G4 (**c**). Lysate was loaded with 20% of the amount of protein used for IP. Arrows indicate specific anti-ATF4 (~40 kDa; **b**) or anti-NPHP6 (~290 kDa; **c**) immunoreactive bands. (**d**) NPHP6 activates ATF4-mediated transcription. The ATF4-expressing plasmid pCEP-ATF4 and the full-length NPHP6-expressing plasmid pCJW206-Cep290 were cotransfected into HEK293T cells to assess their effects on dual luciferase assays reporter activity for the ATF4-responsive reporter pCRE-ATF4X2. The amount of each plasmid is indicated (in μg). Luciferase activity relative to empty vector control is presented in arbitrary units as mean ± s.d. from one typical experiment out of four experiments. (**e**–**g**) Silencing of NPHP6 transcription. (**e**) HEK293T cells transfected with vector pTER (empty), pTER-Luci (for depletion of luciferase, negative control) or pTER-NPHP6 for 48 h were subjected to 3–12% gradient SDS-PAGE followed by immunoblotting to visualize the indicated proteins for efficiency of RNA interference (note that reduction of NPHP6 protein amount occurs only with TER-NPHP6). (**f**) Knocking down NPHP6 attenuates endogenous ATF4-mediated transcription. The indicated plasmids (μg) were cotransfected with the reporter construct into HEK293T cells for 48 h. The relative luciferase activity is presented in arbitrary units as mean ± s.d. from one typical experiment. (**g**) NPHP6 demonstrates both cytoplasmic and nuclear distributions. HEK293T cells were subjected to subcellular fractionations. The indicated proteins were visualized by immunoblotting after 3–12% gradient SDS-PAGE. Mitosin (CENPF) and α-tubulin serve as markers for nuclear and cytoplasmic fractions, respectively. Compared with the cytoplasmic fraction, the nuclear fraction was overloaded by twofold. WCL, whole-cell lysates; CE, cytoplasmic extracts; NE, nuclear extracts.

harboring a 0.35-kb *cep290* cDNA insert that corresponds to the 5′ end of the gene. Whole-mount *in situ* hybridization was performed as described[27].

Zebrafish morpholino injections. Wild-type TL or TÜAB zebrafish were maintained and raised as described[28]. Dechorionated embryos were kept at 28.5 °C in E3 solution with or without 0.003% PTU (1-phenyl-2-thiourea; Sigma) to suppress pigmentation and were staged according to somite number (som) or hours post-fertilization (hpf)[28]. The zebrafish *CEP290* homolog was identified in TBLASTN searches of zebrafish genomic sequence (Sanger Institute) using the human *CEP290* as query. The predicted zebrafish *cep290* sequence was confirmed as the true homolog by reverse BLASTP against GenBank (nonredundant protein). Morpholino oligonucleotides (Gene-Tools) were designed against ATG initiation codon sequence (ATG-MO) and against exon 42 splice donor sequence (SpMO). A mismatch (mm) morpholino served as a negative control (**Supplementary Table 1** online). Morpholinos stocks were dissolved at 2 mM in water and 4.6 nl of injection solution (0.2 M KCl, 0.1% phenol red) containing 0.5 mM *cep290* or mismatch morpholino was injected into fertilized eggs at the one- to two-cell stage using a Nanoliter2000 injector (WPI). Estimated final morpholino cytoplasmic concentration was 9 μM. Both morpholinos resulted in similar frequencies of phenotypic changes (see Results). For acetylated tubulin staining the embryos were fixed in Dent's Fix (80% methanol/20% DMSO) at 4 °C overnight. After rehydration they were washed several times in 1× PBS with 0.5% Tween-20 and blocked in 1× PBS-DBT (1% DMSO/1% BSA/0.5% Tween-20) with 10% normal goat serum (NGS; Sigma) at room temperature for 2 h. Primary antibody incubation in 1× PBS-DBT 10% NGS (1:500 monoclonal anti-acetylated tubulin 6-11B-1 (ref. 29) (Sigma) was at 4 °C overnight. The embryos were washed in 1× PBS with 0.5% Tween-20 and blocked in 1× PBS-DBT 10% NGS at 25 °C for 1 h and then incubated in 1:1,000 goat anti-mouse Alexa 546 (Molecular Probes) in 1× PBS-DBT 10% NGS at 4 °C overnight. After rinsing in 1× PBS the embryos were washed with methanol and equilibrated in clearing solution (one-third benzoyl-alcohol and two-thirds benzoyl-benzoate) and examined using a Bio-Rad Radiance 2000 confocal microscope. *Z* stacks were acquired and used for creation of projections with extended focus. Cilia length was estimated using ImageJ.

Dual luciferase reporter assays, siRNA studies, and subcellular fractionation. The firefly luciferase reporter construct pCRE-ATF4X2 contains two artificial CRE sites upstream of a minimal promoter and was a gift from T. Hai (Department of Molecular and Cellular Biochemistry, Ohio State University). HEK293T cells in six-well plates were cotransfected with 6.1 μg of plasmid mixture per well, including reporter construct (1 μg) and pRL-TK (0.1 μg for each transfection in **Fig. 5d**) for constitutive expression of *Renilla* luciferase (Promega) as an internal control. Cotransfected plasmids are indicated in **Figure 5d**. Luciferase assays were performed using a dual-luciferase reporter assay system (Promega) 48 h after transfection. The ratio of firefly luciferase activity to *Renilla* luciferase activity ('relative luciferase activity') is presented in arbitrary units. For small interfering RNA (siRNA) studies, pTER-NPHP6 was constructed to express an siRNA to repress NPHP6 expression. The target sequence was nucleotides 1272 to 1290 of human *CEP290* cDNA (**Supplementary Table 1** online). For dual luciferase reporter assays HEK293T cells in six-well plates were cotransfected per well with plasmid mixture containing 1 μg of reporter construct, 0.1 μg of pRL-TK and 4 μg of pTER or pTER-NPHP6. Luciferase assays were performed 48 h after transfection. The experiment was repeated for four times. Subcellular fractionation was performed following a protocol at the website of Rockland, Inc. Briefly, cells were lysed in cytoplasmic extract buffer. After spinning at 1,850*g* for 4 min, the supernatant was collected. The remaining pellet was then resuspended in five volumes of detergent-free cytoplasmic extract buffer. Nuclei were centrifuged again and the nuclear extract was obtained from the nuclear preparation.

Accession codes. GenBank: human *CEP290* cDNA, DQ109808 and NM_025114. Accession numbers of NPHP6 orthologs and detailed sequence alignments are available from the authors.

URLs. UCSC Genome Browser: http://genome.ucsc.edu. Rockland, Inc.: http://www.rockland-inc.com/commerce/misc/Nuclear%20Extract.jsp.

For additional methods descriptions, see **Supplementary Methods** online.

Note: Supplementary information is available on the Nature Genetics website.

ACKNOWLEDGMENTS

We sincerely thank the affected individuals and their families for participation. We acknowledge R.H. Lyons for excellent large-scale sequencing. We are grateful to the following physicians for contribution of materials and clinical data from patients: J. Kuehr (Karlsruhe, Germany), B. Polak (University of Rotterdam, The Netherlands), D. Doherty (University of Washington, Seattle) and N. Illum (Odense, Denmark). This research was supported by grants from the US National Institutes of Health to F.H. (DK1069274, DK1068306, DK064614), to A.S. (EY07961 and EY07003), to D.S.W. (EY13408) and to I.D. (DK53093), and by grants to A.S. from the Foundation Fighting Blindness and Research to Prevent Blindness (RPB). F.H. is the Frederick G. L. Huetwell Professor. A.S. is the Harold F. Falls Collegiate Professor and recipient of RPB Senior Scientific Investigator Award. M.R.L. holds Michael Smith Foundation for Health Research (MSFHR) and Canadian Institutes of Health Research (CIHR) scholar awards. The work was further supported by the German Federal Ministry of Science and Education through the National Genome Research Network (G.N., C.B., H.C.H. and P.N.); by grants from the German Research Foundation (A.K.); by the National Science Foundation of China (X.Z., grant numbers 30330330 and 30421005); by the March of Dimes and CIHR (grant CBM134736) (M.R.L.); by a grant from the Michigan Economic Development Corporation, Life Sciences Corridor, to D.G. (MEDC38) and a Vision Research Pre-doctoral Training Grant (B.F.); by a grant from the N.K.F. (N004727) (J.F.O.); by grants from the Japanese Ministry of Education, Culture, Sports, Science and Technology (MEXT) to T.K. (17018018) and to M.T. (16370075) and by a grant from Japan Space Forum to M.T. (h160179). We thank D. Slusarski for providing maternal *pipetail* mutant embryos.

COMPETING INTERESTS STATEMENT

The authors declare that they have no competing financial interests.

Published online at http://www.nature.com/naturegenetics
Reprints and permissions information is available online at http://npg.nature.com/reprintsandpermissions/

1. Hildebrandt, F., Jungers, P., Robino, C. & Grundfeld, J.-P. Nephronophthisis, medullary cystic kidney disease and medullary sponge kidney disease. in *Diseases of the Kidney and Urinary Tract* (ed. Schrier, R.W.) (Lippincott Williams & Wilkins, Philadelphia, 2001).
2. Saraiva, J.M. & Baraitser, M. Joubert syndrome: a review. *Am. J. Med. Genet.* **43**, 726–731 (1992).
3. Hildebrandt, F. *et al.* A novel gene encoding an SH3 domain protein is mutated in nephronophthisis type 1. *Nat. Genet.* **17**, 149–153 (1997).
4. Olbrich, H. *et al.* Mutations in a novel gene, *NPHP3*, cause adolescent nephronophthisis, tapeto-retinal degeneration and hepatic fibrosis. *Nat. Genet.* **34**, 455–459 (2003).
5. Otto, E.A. *et al.* Mutations in *INVS* encoding inversin cause nephronophthisis type 2, linking renal cystic disease to the function of primary cilia and left-right axis determination. *Nat. Genet.* **34**, 413–420 (2003).
6. Otto, E. *et al.* A gene mutated in nephronophthisis and retinitis pigmentosa encodes a novel protein, nephroretinin, conserved in evolution. *Am. J. Hum. Genet.* **71**, 1161–1167 (2002).
7. Otto, E.A. *et al.* Nephrocystin-5, a ciliary IQ domain protein, is mutated in Senior-Loken syndrome and interacts with RPGR and calmodulin. *Nat. Genet.* **37**, 282–288 (2005).
8. Watnick, T. & Germino, G. From cilia to cyst. *Nat. Genet.* **34**, 355–356 (2003).
9. Simons, M. *et al.* Inversin, the gene product mutated in nephronophthisis type II, functions as a molecular switch between Wnt signaling pathways. *Nat. Genet.* **37**, 537–543 (2005).
10. Germino, G.G. Linking cilia to Wnts. *Nat. Genet.* **37**, 455–457 (2005).
11. Hildebrandt, F. & Otto, E. Cilia and centrosomes: a unifying pathogenic concept for cystic kidney disease? *Nat. Rev. Genet.* **6**, 928–940 (2005).
12. Utsch, B. *et al.* Identification of the first *AHI1* gene mutations in families with Joubert syndrome and nephronophthisis. *Pediatr. Nephrol.* **21**, 32–35 (2005).
13. Andersen, J.S. *et al.* Proteomic characterization of the human centrosome by protein correlation profiling. *Nature* **426**, 570–574 (2003).
14. Nasmyth, K. & Haering, C.H. The structure and function of smc and kleisin complexes. *Annu. Rev. Biochem.* **74**, 595–648 (2005).
15. Zhou, X. *et al.* Mitosin/CENP-F as a negative regulator of activating transcription factor-4. *J. Biol. Chem.* **280**, 13973–13977 (2005).
16. Khanna, H. *et al.* RPGR-ORF15, which is mutated in retinitis pigmentosa, associates with SMC1, SMC3, and microtubule transport proteins. *J. Biol. Chem.* **280**, 33580–33587 (2005).
17. Morgan, D. *et al.* Expression analyses and interaction with the anaphase promoting complex protein Apc2 suggest a role for inversin in primary cilia and involvement in the cell cycle. *Hum. Mol. Genet.* **11**, 3345–3350 (2002).

18. Mollet, G. *et al.* The gene mutated in juvenile nephronophthisis type 4 encodes a novel protein that interacts with nephrocystin. *Nat. Genet.* **32**, 300–305 (2002).
19. Chen, D. & Shou, C. Molecular cloning of a tumor-associated antigen recognized by monoclonal antibody 3H11. *Biochem. Biophys. Res. Commun.* **280**, 99–103 (2001).
20. Vaughan, K.T. & Vallee, R.B. Cytoplasmic dynein binds dynactin through a direct interaction between the intermediate chains and p150Glued. *J. Cell Biol.* **131**, 1507–1516 (1995).
21. Kim, J.C. *et al.* MKKS/BBS6, a divergent chaperonin-like protein linked to the obesity disorder Bardet-Biedl syndrome, is a novel centrosomal component required for cytokinesis. *J. Cell Sci.* **118**, 1007–1020 (2005).
22. Mollet, G. *et al.* Characterization of the nephrocystin/nephrocystin-4 complex and subcellular localization of nephrocystin-4 to primary cilia and centrosomes. *Hum. Mol. Genet.* **14**, 645–656 (2005).
23. Pazour, G.J. & Witman, G.B. The vertebrate primary cilium is a sensory organelle. *Curr. Opin. Cell Biol.* **15**, 105–110 (2003).
24. Kramer-Zucker, A.G. *et al.* Cilia-driven fluid flow in the zebrafish pronephros, brain and Kupffer's vesicle is required for normal organogenesis. *Development* **132**, 1907–1921 (2005).
25. Mazet, F. *et al.* Molecular evidence from Ciona intestinalis for the evolutionary origin of vertebrate sensory placodes. *Dev. Biol.* **282**, 494–508 (2005).
26. Nakashima, Y. *et al.* Origin of the vertebrate visual cycle: genes encoding retinal photoisomerase and two putative visual cycle proteins are expressed in whole brain of a primitive chordate. *J. Comp. Neurol.* **460**, 180–190 (2003).
27. Barthel, L.K. & Raymond, P.A. In situ hybridization studies of retinal neurons. *Methods Enzymol.* **316**, 579–590 (2000).
28. Westerfield, M. *The Zebrafish Book* (University of Oregon Press, Portland, Oregon, 1995).
29. Piperno, G. & Fuller, M.T. Monoclonal antibodies specific for an acetylated form of alpha-tubulin recognize the antigen in cilia and flagella from a variety of organisms. *J. Cell Biol.* **101**, 2085–2094 (1985).
30. Khanna, H. *et al.* Early-onset retinal degeneration in the *rd16* mouse is associated with an in-frame deletion in the novel centrosomal protein CEP290 (NPHP6) that interacts with retinitis pigmentosa GTPase regulator (RPGR). *Hum. Mol. Genet.* (in the press).